Performance Improvement of the CRJ700 Aircraft Using Adaptive Winglets with Variable Twist Angle

Léo RONGIÈRES[1,a], Ruxandra Mihaela BOTEZ[1,b]

*Corresponding author
[1]University of Quebec, École de Technologie Supérieure, Laboratory of Applied Research in Active Controls, Avionics and AeroServoElasticity LARCASE, Montreal Quebec, H3C-1K3,
Ruxandra.Botez@etsmtl.ca

DOI: 10.13111/2066-8201.2026.18.1.8

Received: 21 January 2026/ Accepted: 20 February 2026/ Published: March 2026

Abstract: *This study investigates the potential of adaptive winglets with variable twist angles to improve the aerodynamic and energy performance of the Bombardier CRJ700. CFD simulations conducted in Star-CCM+, validated with a level-D flight simulator at LARCASE, reveal that twist adaptation can significantly reduce drag. A trajectory-based performance analysis shows that, during climb, adaptive winglets can reduce fuel consumption and climb time by up to 1.24% and 1.82%, respectively, or an increase of the ground distance by up to 2.67%. In cruise, fuel savings reach up to 0.4%. These results highlight the effectiveness of adaptive winglets in enhancing regional jet efficiency.*

Key Words: *adaptive winglets, CFD simulations, aircraft aerodynamic performance, aerodynamic coefficients*

NOMENCLATURE

C_L	=	lift coefficient
C_D	=	drag coefficient
C_M	=	pitch momentum coefficient
ξ	=	winglet twist angle
α	=	angle of attack
M	=	Mach number
ϵ	=	downwash angle
F_N	=	thrust
W_f	=	fuel flow
RoC	=	rate of climb
ρ	=	density

Subscripts

wb	= wing-body
ht	= horizontal tail
s	= overall aircraft

[a] M.Sc.A. Student, ETS, LARCASE, 1100 Dame West, Montreal, QC, H3C-1K3, Canada
[b] Full Professor, AIAA Associate Fellow, Canada Research Chair Holder Level 1 in Aircraft Modeling and Simulation, Head of the LARCASE, ETS, 1100 Dame West, Montreal, QC, H3C-1K3, Canada

I. INTRODUCTION

The aerospace industry represents a critical component of global transportation while facing substantial environmental and economic challenges. As air traffic continues to grow, fuel consumption and greenhouse gas emissions have emerged as primary concerns within the sector. Enhancing aircraft aerodynamic performance has become an essential approach for reducing environmental impact and improving energy efficiency.

Among potential technological solutions, adaptive winglets capable of modifying their geometry according to flight conditions are attracting growing interest. These advanced devices enable real-time optimization of aerodynamic performance through lift increase and drag reduction. Consequently, research into their impact on overall aircraft performance, particularly on fuel efficiency and climb phase duration, constitutes a strategic priority for the aerospace industry.

A. Literature Review

Adaptive winglets significantly improve aircraft performance by optimizing lift, drag, and energy efficiency through geometric morphing including cant angle, span, sweep, and twist. Current research focuses primarily on single-variable systems due to structural constraints such as multi-parameter modifications that often cancel potential aerodynamic benefits [1].

The cant angle remains the most studied parameter. A study conducted on the Bombardier CRJ700 showed a 4-6% fuel savings during its climb phases with cant angle optimization [2], using results from Computational Fluid Dynamics (CFD). Winglet twist also shows promising results, demonstrating measurable variations in lift ($\Delta_{\%}C_L = 3.3\%$) and drag coefficients ($\Delta C_D = 0.003$) at different angles [3] for the wing of an UAV using the Vortex Lattice Method (VLM).

Span and sweep angles also affect significantly the performance, with drag reductions up to $\Delta C_D = 0.001$ in certain configurations [4]. To study the winglets aerodynamics, CFD using Reynolds-Averaged Navier–Stokes (RANS) equations provides the best balance between accuracy and computational cost, with the $k-\omega$ Shear Stress Transport (SST) model proving to be particularly effective for CRJ700 simulations [5].

While higher-fidelity methods, such as LES and DES capture unsteady phenomena, their computational expense limits their application. The VLM serves very well for preliminary studies despite not capturing parasitic drag [6], while wind tunnel testing remains essential for experimental validation.

Performance evaluation typically relies on integrated flight dynamics models to optimize adaptive winglets across different flight phases [7]. A study on the CRJ700 assessed performance during climb phases by discretizing the trajectory, and by integrating variables such as fuel flow and rate of climb [2], allows for a comprehensive evaluation of total performance gains. Adaptive winglets also demonstrated promising results under crosswind conditions, which are particularly significant at low Mach numbers [8].

B. Paper Objectives

The main objective of this paper is to evaluate the performance of adaptive winglets with variable twist angles for the Bombardier CRJ700 aircraft. This research examines how this adaptative winglets technology can improve aircraft performance through detailed analysis of its aerodynamic impact and evaluation across multiple flight trajectories.

A high-fidelity aerodynamic model was developed using CFD in Star-CCM+ and validated with the Virtual Research Simulator (VRESIM), present at the Laboratory of Applied Research in Active Controls, Avionics and AeroServoElasticity (LARCASE). As

shown in Fig. 1 this Level D-certified simulator (the highest certification level from the FAA) was developed by CAE Inc. specifically for LARCASE research needs, enabling high-precision flight simulations.

This model was then used to measure variations in the adaptive winglet's aerodynamic coefficients with the winglet's twist angle.

Fig. 1 Bombardier CRJ700 Level D Simulator at LARCASE

Using the CFD results, simulations compared configurations with and without adaptive winglets across different flight trajectories. These comparisons focused on three key parameters: fuel consumption, climb time, and ground distance traveled. The study employed LARCASE's performance model developed from VRESIM data for these simulations. Finally, the results were synthesized to provide recommendations for optimizing adaptive winglets and their potential aerospace applications.

II. METHODOLOGY: ADAPTIVE WINGLET ANALYSIS

To evaluate the aerodynamic impact of integrating adatative winglets on a regional jet, a custom variable twist angle winglet was developed specifically for the CRJ700. Using a high-resolution aerodynamic simulation framework, this study examined how variations in winglet twist influence key aerodynamic coefficients (including lift, drag, and pitch moment) across a range of flight conditions and adaptative winglets configurations. This approach enables a comprehensive assessment of both the potential gains and trade-offs associated with adaptive winglets use.

A. Adaptive Winglet Design

The type of adaptive winglet studied modifies the twist angle, denoted by ξ. The original CRJ700 3D aerodynamic model was modified to create a geometry capable of changing this twist angle.

The twist angle ξ corresponds to the angle of incidence of the airfoil located at the winglet tip. The cross-sections are defined perpendicularly to the dihedral angle (inclination angle relative to the horizontal), as illustrated in Fig. 2a. The root of the winglet was chosen just after the transition zone between the wing and the winglet. The base section is fixed, while the tip section rotates according to the twist angle ξ, as shown in Fig. 2b.

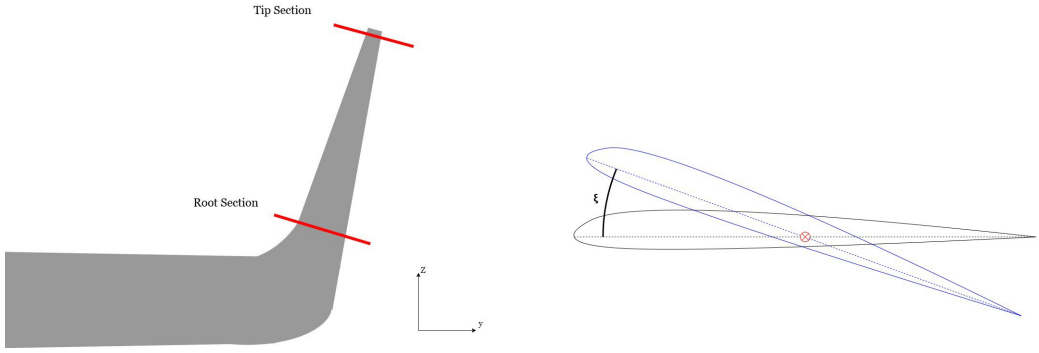

a) Sections selected as endpoints of the variable twist system

(b) Twist angle ξ

Fig. 2 Illustrative diagrams of the variable twist angle

A parametric 3D model was developed to allow the twist angle variation, using the diagrams described previously. Figure 3 illustrates the winglet in three different configurations: a twist angle of $\xi = 20^{\circ}$, the reference twist angle corresponding to the original CRJ700 winglet ($\xi = -2.67^{\circ}$), and a twist angle of $\xi = -20^{\circ}$.

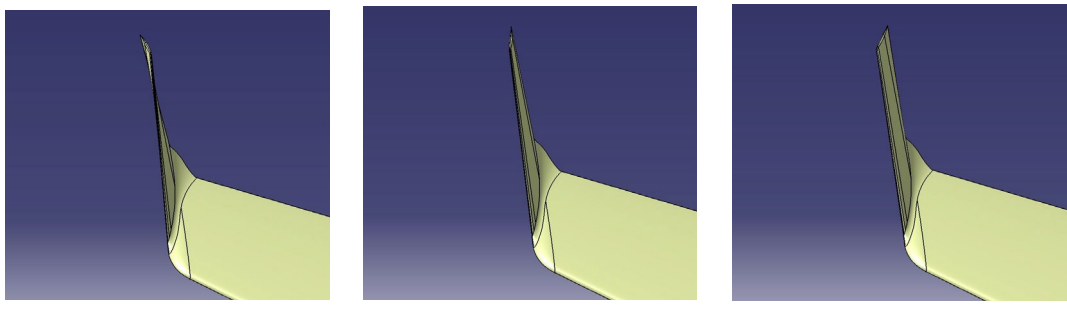

(a) $\xi = 20^{\circ}$ (b) $\xi = -2.67^{\circ}$ (reference) (c) $\xi = -20^{\circ}$

Fig. 3 Configurations of the adaptive winglet for different twist angles

B. Aerodynamic Model

To investigate the aerodynamic behavior introduced by the morphing capability of the adpatative winglet, a detailed CFD model was created using STAR-CCM+. This analysis used the validated aerodynamic setup initially developed for the baseline Bombardier CRJ700 configuration, which was then adapted to simulate the aircraft modified with the variable-geometry winglet.

1. Mesh Design

The generation of a high-quality mesh is a critical prerequisite for accurate CFD simulations. In this study, a polyhedral mesh was developed for the Bombardier CRJ700 using STAR-CCM+, with a focus on achieving a balance between geometric fidelity, numerical accuracy, and computational efficiency.

The computational domain was constructed in accordance with best practices in aerodynamics. It represents five fuselage lengths upstream, ten downstream, and spans eight times the wingspan laterally and vertically. The origin of the reference frame was placed at the aircraft's nose tip to provide a consistent geometric reference. Boundary conditions were

assigned as follows: a velocity inlet upstream, a pressure outlet downstream, and symmetry-type slip walls on lateral boundaries. Preliminary sensitivity analyses confirmed that this configuration adequately minimizes the influence of far-field boundaries on the near-body flow solution.

A polyhedral mesh was selected due to its superior performance on complex geometries compared to structured or tetrahedral meshes. It enables efficient local refinement and robust control over near-wall resolution. Near-wall prism layers were generated to obtain the boundary layer, targeting a non-dimensional wall distance y^+ between 100 and 200. This range is optimal for wall-function-based turbulence modeling and ensures accurate capture of velocity and pressure gradients without excessively increasing the cell count.

Additional mesh refinements was performed in high-gradient regions, such as the fuselage, wing surfaces, leading and trailing edges, and the wake. The wake refinement was dynamically aligned with the flow direction to ensure accurate resolution of vortex structures. Cone-shaped volumetric refinements were also employed near critical leading and trailing edge regions to enhance resolution of flow separation and pressure gradients.

The final mesh contains approximately 38 million cells. The wall-adjacent cells exhibit a y^+ distribution between 50 and 180, which ensures their compatibility with the selected turbulence model. Mesh quality metrics were evaluated following STAR-CCM+ guidelines. The maximum cell distortion angle is 70.8°, remaining well below the 85° threshold commonly accepted for stable numerical performance. The cell quality metric, ranging from 0.15 to 1.00 with an average of 0.60, remains within acceptable limits for polyhedral grids. Furthermore, 99.58% of cells exhibit a volume change between 10% and 100%, supporting smooth transitions and minimizing numerical dissipation.

In summary, the generated mesh satisfies all the criteria for high-fidelity aerodynamic simulation and provides a robust foundation for the analyses presented in the following sections.

2. Simulation Settings

The aerodynamic simulations were performed in the compressible flow regime using the RANS equations, with both the flow and energy equations solved in a fully coupled manner. The working fluid was treated as an ideal gas used to accurately capture compressibility effects. Given the high Reynolds numbers involved ($Re > 10^7$), the flow was assumed fully turbulent, eliminating the need for its transition modeling.

For turbulence closure, the k–ω SST model was employed. This hybrid model blends the near-wall resolution strength of the k–ω formulation with the robustness of k–ε in the free-stream, offering improved accuracy in boundary-layer separation and adverse pressure gradient scenarios. Its selection was performed by prior comparative studies on the CRJ700 airframe [2], where it outperformed simpler alternatives in accuracy, such as Spalart–Allmaras.

The turbulent inflow parameteres, specifically the turbulent kinetic energy k and the specific dissipation rate ω, were initialized using semi-empirical formulas. These parameters were estimated with the Eqs. (1):

$$k = \left(\frac{\nu}{l}\right)^2, \qquad \omega = \frac{k}{l} \tag{1}$$

where ν is the kinematic viscosity and l is the turbulence length scale, considered here as the mean aerodynamic chord of the CRJ700. This initialization enhances the model convergence and ensures a physically consistent turbulence field at the domain boundaries [9]. In terms of

transport properties, the dynamic viscosity μ was calculated using Sutherland's law to account for temperature-dependent variation, a critical factor in compressible regimes. Its expression is given by the Eq. (2).

$$\mu(T) = \frac{A_s\sqrt{T}}{1+\frac{T_s}{T}} \tag{2}$$

where T is the absolute temperature in Kelvin, $A_S = 1.458\times10^{-6}$ kgm^{-1} s^{-1} K$^{-1/2}$ and $T_s = 110.4$K are air empirical constants. This formulation ensures accurate modeling of thermoviscous effects in boundary layers.

The numerical implementation of these models was conducted within the STAR-CCM+ solver, leveraging its advanced capabilities for coupled flow, thermodynamics, and turbulence modeling. This comprehensive framework ensures reliable prediction of aerodynamic forces and flow behavior for various configurations investigated in this study.

3. Validation

CFD simulations were performed for five flight conditions defined from flight plans extracted from the VRESIM simulator, covering a range of altitudes and Mach numbers encountered by the CRJ700 during its typical operations.

The flight conditions expressed in terms of altitudes and Mach number for various angles of attack are summarized in Table 1.

Table 1. Flight conditions studied and associated angles of attack

No.	Altitude (ft)	Mach Number	Angles of attack (°)
1	5000	0.31	
2	10000	0.45	
3	20000	0.54	-2, -1, 0, 1, 2, 3, 4
4	25000	0.66	
5	30000	0.79	

The convergence of the CFD solutions was monitored through the flow equations residuals. Typically, between 1000 and 1300 iterations were required for residuals to drop below a threshold of 10^{-4}, ensuring numerical stability and reliable results. No significant fluctuations were observed beyond this point, confirming steady-state model convergence.

The aerodynamic coefficients of the lift (C_L), drag (C_D), and pitching moment (C_M) extracted from CFD results were compared with those obtained from the VRESIM simulator.

The statistical analysis of the results has shown in the Fig. 4 that the lift coefficient C_L was estimated with an error margin of -0.0019 ± 0.0146 (95% confidence interval). Similarly, the drag coefficient C_D displayed an error of -0.00018 ± 0.00110, while the pitching moment coefficient C_M showed a precision of -0.00192 ± 0.00168. These low errors confirm the reliability of the developed aerodynamic model, validated across the entire simulated flight envelope for Mach numbers ranging from 0.31 to 0.79.

Based on this validation, the aerodynamic model of the Bombardier CRJ700 can be considered accurate. Consequently, all its parameters, assumptions, and configurations were used to compute the aerodynamic characteristics of the aircraft equipped with adaptive winglets.

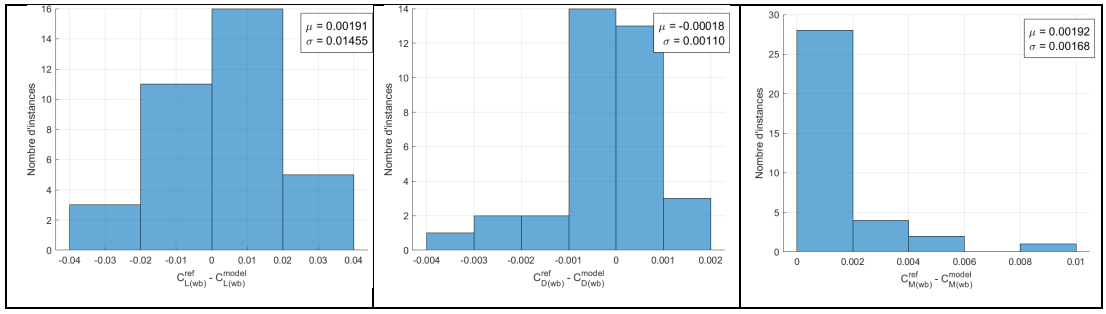

a) Distribution of C_L errors (b) Distribution of C_D errors (c) Distribution of C_M errors

Fig. 4 Gaussian distributions of errors between CFD and VRESIM aerodynamic coefficients

4. Downwash Angle Calculation Method

The downwash angle was evaluated by measuring the difference in the orientation of the flow velocity vector upstream and downstream of the wing. This analysis is based on the velocity components (U_x, U_y, and U_z) obtained after convergence of the STAR-CCM+ simulations.

For each simulated configuration, twenty probes $P_i(x, y, z)$ were strategically positioned to capture the evolution of the velocity field. Seven of these probes (P_1 to P_{10}) were located upstream of the wing, while the remaining ten probes (P_{11} to P_{20}) were placed downstream (Fig. 5). These velocity sensors were spaced laterally by 1 m. Thus, probes P_1 and P_{10} were closest to the fuselage axis at 1.5 m, whereas probes P_{11} and P_{20} were positioned at 10.5 m, covering a wide lateral portion of the flow.

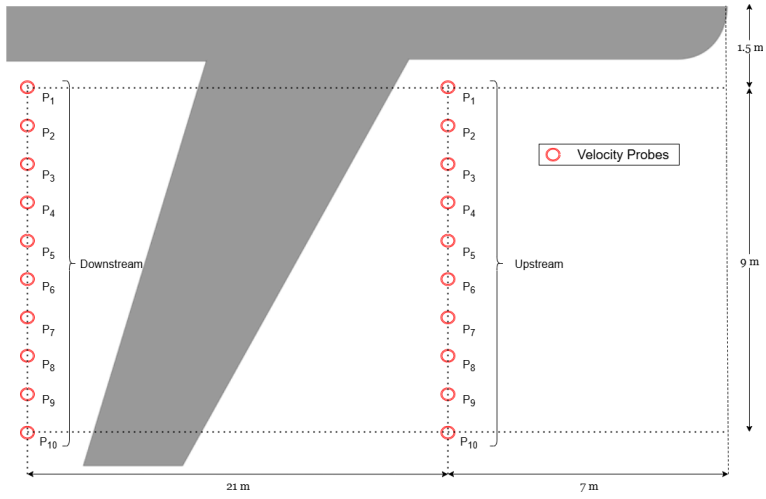

Fig. 5 Placement of velocity probes for measuring the downwash angle

The average downwash angle ϵ was determined according to Eq. (3), where $\tan^{-1}$ denotes the arctangent function, and U_z and U_x are the vertical and horizontal components of the velocity, respectively. The subscripts "upstream" and "downstream" distinguish the measurements of the velocity probes located before and after the wing, as shown in the next Eq. (3):

$$\epsilon = \frac{1}{10}\sum_{1=1}^{10}\left[\tan^{-1}\left(\frac{U_z(i)}{U_x(i)}\right)_{downstream} - \tan^{-1}\left(\frac{U_z(i)}{U_x(i)}\right)_{upstream}\right] \quad (3)$$

To validate this methodology, the calculated downwash angles were compared with VRESIM angles. Figure 6 shows the distribution of errors for the downwash angle ϵ. The mean error is 0.16719°, with a standard deviation of 0.09378°. The minimum error deviation is 0.00577° and the maximum error deviation is 0.37144°. This relatively large dispersion indicates a low precision of this method, with a tendency to overestimate the downwash angle ϵ.

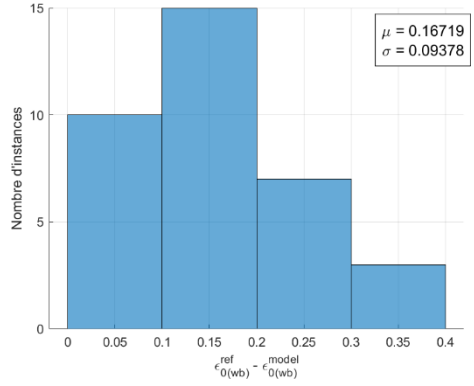

Fig. 6 Distribution of errors calculated by CFD and using the VRESIM simulator for the downwash angle ϵ

C. Aerodynamic Simulations Results

The longitudinal aerodynamic coefficients (C_L, C_D, and C_M) were obtained for various twist angles ξ, Mach numbers M and angle of attack α. Figure 7 presents their variations for $\alpha = 0°$ through three subfigures, along with polynomial regression fits. The polynomial regressions for C_L, C_D, and C_M are given in Eq. (4), where a_{ij} are the polynomial coefficients, while M and ξ represent the Mach number and twist angle, respectively:

$$C_{L,D,M}(M,\xi) = \sum_{i=0}^{m}\sum_{j=0}^{n} a_{ij} M^i \xi^j \tag{4}$$

For all three longitudinal aerodynamic coefficients, the regressions with R^2 closest to 1 ($R^2 > 0.98$) corresponded to 4th order polynomials for both Mach numbers and twist angles. The lift coefficient C_L increases with the twist angle up to a maximum located between 10° and 15°, while the drag coefficient C_D shows a minimum between − 12° and 5°.

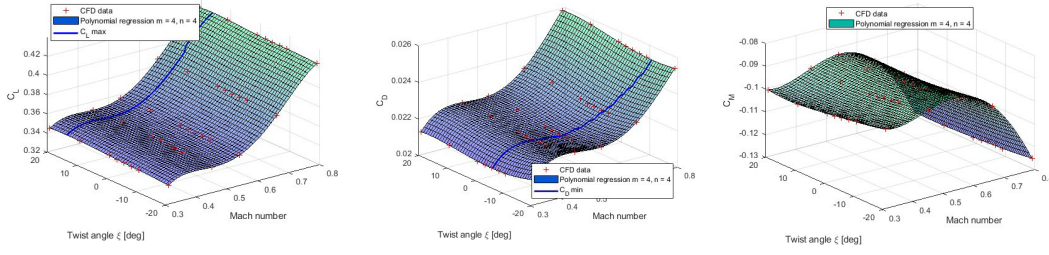

(a) Lift coefficient C_L (b) Drag coefficient C_D (c) Pitching moment C_M

Fig. 7 Variations of aerodynamic coefficients as a function of twist angle and Mach number at $\alpha = 0°$

Figure 8a shows the relative error of the drag coefficient as a function of the twist angle ξ, compared to the reference configuration ($\xi = -2.67°$), for five Mach numbers at $\alpha = 0°$. A negative

deviation corresponds to a drag reduction. For lower Mach numbers (M = 0.31 to M = 0.54), the improvements remain marginal, while for higher Mach numbers (M = 0.66 and M = 0.79), more noticeable drag reductions are observed, reaching up to 0.4%. However, drag increases at large twist angles (−20° and 20°).

Figure 8b presents the relative errors of the lift coefficient. For all Mach numbers, the lift coefficient increases with the twist angle ξ, reaching a maximum of approximately 0.5%, before decreasing. Additionally, the variations in lift are less pronounced at higher Mach numbers.

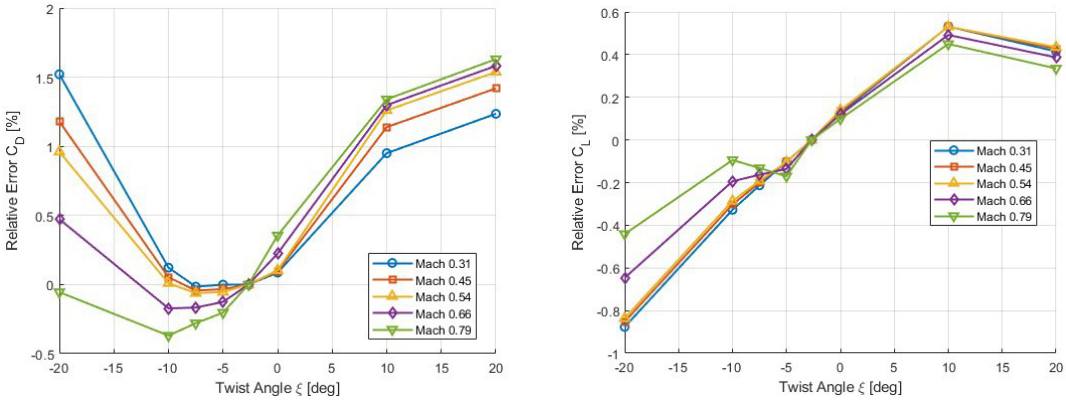

(a) Relative error of drag coefficient CD (b) Relative error of lift coefficient CL

Fig. 8 Relative error of aerodynamic coefficients as a function of twist angle for different Mach numbers at $\alpha = 0^{\circ}$

III. GLOBAL PERFORMANCE IMPROVEMENT

A. Performance Model

This section details the methodology used to evaluate the performance of adaptive winglets by simulating flight trajectories using the model developed at the LARCASE laboratory.

1. Aerodynamic Model

The aerodynamic forces (L, D) and pitching moment (M) acting on an aircraft are determined with the lift (C_L), drag (C_D), and pitching moment (C_M) coefficients. These coefficients are calculated via the following equations:

$$L = \frac{1}{2}\rho S V^2 C_{L_s}(\alpha, M, \delta_{stab}, \delta_{elev}) \tag{5}$$

$$D = \frac{1}{2}\rho S V^2 C_{D_s}(\alpha, M, \delta_{stab}, \delta_{elev}) \tag{6}$$

$$M = \frac{1}{2}\rho S V^2 \bar{c} C_{M_s}(\alpha, M, \delta_{stab}, \delta_{elev}) \tag{7}$$

where ρ is air density, S is the wing reference area, V is true airspeed (TAS), $\bar{c}$ is the mean aerodynamic chord (MAC), α is the angle of attack, and M is the Mach number. C_L, C_D, and C_M depend on flight conditions (α and M), the deflection angles of the longitudinal control surfaces (stabilizer δ_{stab} and elevators δ_{elev}). Low-speed maneuvers (takeoff and landing) are not considered, thus flaps and slats are assumed retracted. Only longitudinal control surfaces are

studied, excluding rudders, ailerons, and spoilers.

To integrate the aerodynamic model into the complete aircraft model, the aerodynamic contributions of the airframe (wb) (wing and fuselage) and horizontal tail (ht) (stabilizer) are considered separately. Simulating diverse flow conditions for various winglet twist angles to evaluate their contributions would require significant computational time. Therefore, to minimize costs, the methodology chosen in this paper calculates the global aerodynamic coefficients (C_{L_s}, C_{D_s}, and C_{M_s}) using the following equations:

$$C_{L_s} = C_{L_{(wb)}} + \frac{S_{ht}}{S_{wb}}\left[C_{L_{(ht)}}\cos(\epsilon) - C_{D_{(ht)}}\sin(\epsilon)\right] \tag{8}$$

$$C_{D_s} = C_{D_{(wb)}} + \frac{S_{ht}}{S_{wb}}\left[C_{D_{(ht)}}\,cos(\epsilon) + C_{L_{(ht)}}\,sin(\epsilon)\right] \tag{9}$$

$$\begin{aligned} C_{M_s} = C_{M_{(wb)}} &+ \frac{S_{ht}z_{ht}}{S_{wb}\bar{c}}\left[C_{D_{(ht)}}\,cos(\epsilon) - C_{L_{(ht)}}\,sin(\epsilon)\right] \\ &- \frac{S_{ht}x_{ht}}{S_{wb}\bar{c}}\left[C_{L_{(ht)}}\cos(\epsilon) + C_{D_{(ht)}}\sin(\epsilon)\right] \end{aligned} \tag{10}$$

where S_{wb} and S_{ht} denote the reference areas of the wing-body and horizontal tail, respectively. Subscripts wb, ht, and s refer to the aerodynamic contributions of the wing-body, horizontal tail, and overall aircraft in the stability axis, z_{ht} and x_{ht} are the Cartesian projections of the distance between the aerodynamic centers of the wing and horizontal tail, while the downwash angle ϵ corresponds to the flow deflection angle caused by the wing. This angle depends on the airframe geometry, meaning the horizontal tail interacts with the flow at an angle of $\alpha - \epsilon + \delta_{\text{stab}}$ (where δ_{stab} is the stabilizer angle relative to the fuselage line). To distinguish between the wing-body (wb) and horizontal tail (ht) contributions, the downwash angle ϵ must be known. The coefficients and geometric parameters of the horizontal tail were determined in previous studies at the LARCASE laboratory [2]. The measured discrepancies between simulator data and the studied model results were small ($\Delta C_{LS} = 0.007 \pm 0.045$, $\Delta C_{DS} = 0.00015 \pm 0.0014$, $\Delta C_{MS} = -0.0077 \pm 0.0079$).

2. Flight Trajectories Studied

To accurately assess the climb and cruise performance of a regional aircraft equipped with fixed or adaptive winglets, it is essential to understand the standard procedures applicable to this type of aircraft. These procedures have been analyzed in this study. Figure 9 illustrates the complete flight profile for climb and cruise phases.

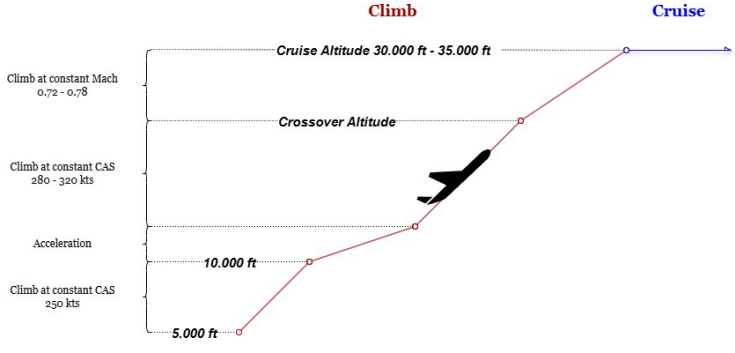

Fig. 9 Complete flight profile for climb and cruise phases

For cruise phases, the altitude and Mach number are assumed constant throughout the flight. For climb segments, flight profiles are defined from the altitude where flaps are fully retracted (typically around 5.000 feet) up to the cruise altitude, which ranges between 30.000 and 35.000 feet for this aircraft [10].

The standard climb protocol for the CRJ-700 follows precise steps, as shown in Fig. 9. According to the aviation authority standards, the aircraft must first climb at a constant Calibrated Air Speed (CAS) of 250 knots until reaching 10.000 feet. It then accelerates from 250 knots to its planned cruise speed, typically between 280 and 320 knots (depending on the crew operation manual).

During this acceleration phase, a vertical speed of 1.000 feet per minute is generally maintained. Two constant-speed flight segments are then executed by the pilot: the first segment is flown at a fixed CAS until the "crossover" altitude, and the second segment is flown at a constant Mach number until the final cruise altitude [10].

3. Performance Model Developed at LARCASE Laboratory

To evaluate aircraft performance during climb and/or cruise phases, a flight segment discretization model has been implemented. Tis discretization method varies with the type of flight segment (e.g., constant acceleration climb, constant speed climb, cruise, etc.). For constant speed climb phases (either CAS or Mach), segments are discretized every 1.000 feet. For acceleration climb segments, the Euler integration is applied every 2 seconds [11]. At each discretization point, flight conditions (altitude, speed, weight, etc.) evolve, leading to an update of the aircraft's state.

This aircraft state corresponds to the necessary control surface configuration needed to ensure static equilibrium under the given flight conditions.

The performance model used in this study, illustrated in Fig. 10, was developed and validated at our LARCASE laboratory [11]. This model calculates various outputs, such as angle of attack (α), required thrust (F_N), stabilizer (δ_{stab}) and elevator (δ_{elev}) angles, fuel flow (W_f), and rate of climb (RoC).

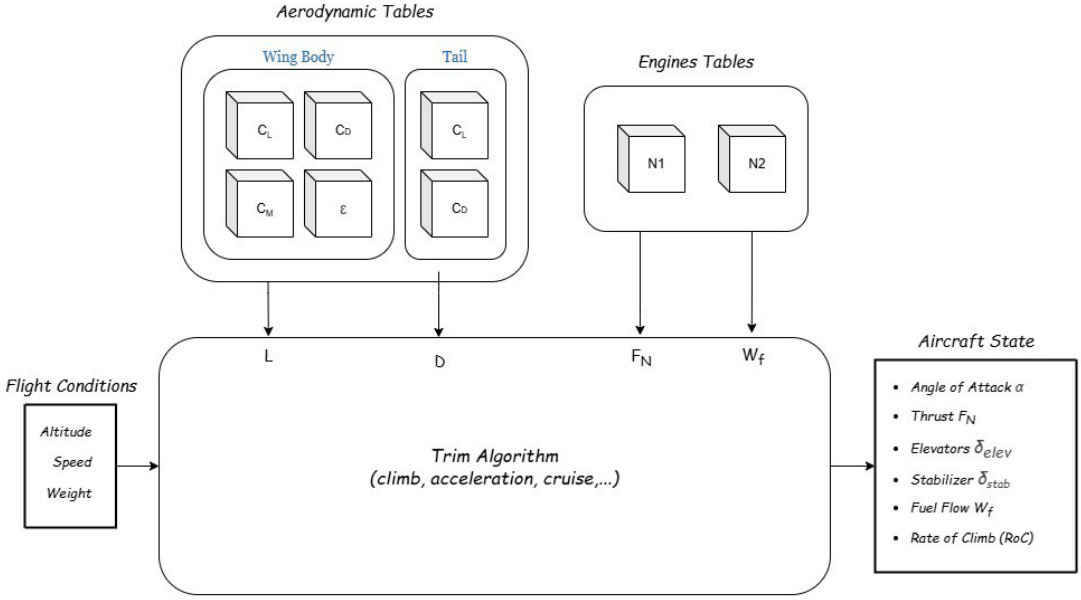

Fig. 10 LARCASE performance model schematic

Throughout the flight, the pilot continuously adjusts lift surfaces and thrust lever angle (TLA) to optimize flight efficiency. The performance model (Fig. 10) simulates these adjustments by predicting the aircraft's static state for given flight conditions using a trim function.

The trim function manages all parameters necessary for the aircraft's static equilibrium, including the angle of attack, vertical flight path angle, positions of longitudinal control surfaces (stabilizers, elevators, etc.), and thrust. For an aircraft to be considered trimmed, all forces and moments projected in a Cartesian coordinate system must obey Newton's second law (Eq. (11)). Winds are neglected in this study, simplifying the trim algorithm. The trim function is expressed by:

$$\text{Trim Function}\begin{cases}\sum \vec{F}_x = m\vec{a}_x \\ \sum \vec{F}_z = m\vec{a}_z \\ \sum \vec{M}_y = \vec{0}\end{cases} \Rightarrow \begin{cases}F_N \sin(\alpha+\phi_T) - D - mg\cos(\gamma) = 0 \\ F_N \cos(\alpha+\phi_T) - L - mg\sin(\gamma) = m\dot{V}_T \\ M_{aero} - M_{engine} = 0\end{cases} \tag{11}$$

where F_N is thrust force, ϕ_T is the engine inclination angle (relative to the body axis), V_T is true airspeed (TAS), m is mass, g is the gravity, γ is the flight path angle, and α is the angle of attack. M_{aero} and M_{engine} are aerodynamic and engine moments, respectively. L and D are the total lift and drag forces, dependent on angle of attack α, stabilizer angle, δ_{stab}, and aircraft true airspeed (TAS) (i.e., Eq. (5)), (6), (8) and (9)).

The trim algorithm solves Eq. (11) by adjusting parameters α, δ_{stab}, and F_N to balance forces and moments under corresponding flight conditions. During climb, TLA is set to "Maximum Climb Thrust Position (MCLT)", meaning that F_N remains at its maximum value for a given flight condition, which allows to calculate the best combinations of parameters α, δ_{stab}, and γ that trim the aircraft during climb.

The performance model is adaptable to different aircraft types, as it uses two types of lookup tables: one table for aerodynamic characteristics (lift, drag, and moment coefficients) and another table for engine parameters (Fig. 10). These aerodynamic tables calculate forces and moments acting on the aircraft based on flight conditions.

Engine data are processed through two distinct lookup tables: one table for thrust (F_N) and the other table for fuel flow (W_f).

These tables calculate altitude (h), Mach number (M), temperature deviation from standard atmosphere (ISA) (ΔISA), fan rotation speed ($N1$), and Thrust Rating Parameter (TRP), as shown in Eq. (12) and (13).

$$F_N = \text{f}(h, M, \Delta ISA, N1(TRP)) \tag{12}$$

$$W_f = f(h, M, \Delta ISA, N1(TRP)) \tag{13}$$

There are six aerodynamic tables. The first three tables correspond to the lift ($C_{L(wb)}$), drag ($C_{D(wb)}$), and pitching moment ($C_{M(wb)}$) coefficients of the wing and fuselage. These tables require wing angle of attack (α_{wb}) and Mach number (M) as inputs (Eq. (14)).

$$\left[C_{L(wb)}, C_{D(wb)}, C_{M(wb)}\right] = f(\alpha_{wb}, M) \tag{14}$$

The next two tables concern the aerodynamic contributions of the horizontal tail, with its lift ($C_{L(ht)}$) and drag ($C_{D(ht)}$) coefficients. They require values of α_{wb}, M, and elevator deflection (δ_{elev}), as shown in Eq. (15).

$$\left[C_{L(ht)}, C_{D(ht)}\right] = f(\alpha_{ht}, M, \delta_{elev}) \quad (15)$$

The sixth and final table provides downwash angle (ϵ) values as a function of wing angle of attack (α_{wb}) and Mach number (M).

$$\epsilon = f(\alpha_{wb}, M) \quad (16)$$

The information in the aerodynamic tables must be as accurate as possible, highlighting the importance of a reliable data source. To develop and validate this performance toolbox, the LARCASE team used aerodynamic and engine data provided by the Bombardier CRJ700 VRESIM flight simulator.

The FAA Level D certified flight simulator provides remarkably accurate data, with an error of less than 5% compared to real flights. To validate the aircraft performance model, simulations were conducted for 60 climb scenarios.

Prediction errors, based on their Gaussian distribution, were $-0.23 \pm 0.52\%$ for climb time, $-0.32 \pm 0.61\%$ for ground distance, and $-0.33 \pm 0.54\%$ for fuel consumption [11]. Cruise accuracy was confirmed by full flight simulations, with an error in fuel consumed less than 2%, suggesting an even smaller error for the cruise phase alone.

These results attest to the model's high precision, making it reliable for evaluating the performance of an aircraft with adaptive winglets.

The performance model used in this study was initially developed within our laboratory, LARCASE, as part of previous work.

Since the primary objective of this thesis is to highlight the performance of an aircraft equipped with adaptive winglets, the model description has been synthesized. For an in-depth explanation of the trim algorithms and trajectory prediction methods integrated into the model, as well as for experimental validation results, the reader is invited to consult the references ([12], [11], [13]).

B. Trajectory Simulation Results

This section presents the results of the aerodynamic study conducted on the integration of an adaptive winglet on a Bombardier CRJ700. To analyze the potential benefits of this modification, the aircraft's performance with adaptive winglets as well as with a fixed winglet (corresponding to the original configuration) was evaluated by simulating various climb and cruise scenarios.

1. Climb Results

Different climb segments were simulated based on the reference aircraft's flight envelope. To better illustrate the results, a specific scenario was analyzed in detail before generalizing the results.

The results obtained for a calibrated airspeed of 320 knots and a Mach number of 0.78 are illustrated in Fig. 11a.

Three strategies were compared: the adaptive winglet strategy minimizing climb time (blue), the adaptive winglet strategy maximizing horizontal distance traveled (green), and the reference profile with fixed winglets (black).

The engine thrust was maintained in the "maximum climb" mode for all configurations. Thus, the observed differences between the trajectories are solely due to changes in aerodynamic coefficients induced by the adaptive winglets.

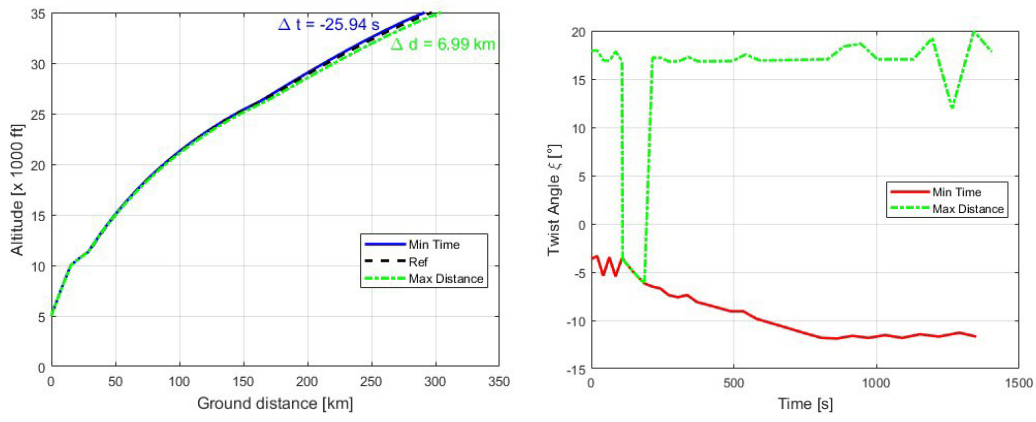

(a) Trajectories (b) Twist angle variations ξ

Fig. 11 Performance results of the climb scenario for the CRJ700 model equipped with fixed and adaptive winglets

The profiles show significant differences beyond the crossover altitude, while trajectories remain relatively close below this threshold. With the time-optimized climb strategy (blue curve), the cruise altitude was reached 25.94 seconds earlier than in the reference case, representing an improvement of 1.89%. In contrast, the horizontal-distance-optimized strategy (green curve) allowed a gain of 6.99 km compared to the reference profile, i.e., a 2.35% increase.

Figure 11b illustrates the variations of the optimal winglet twist angle during the climb. It was observed that, for a rapid climb, the twist angle varies mainly between $-2°$ and $13°$.

Table 2. Parameters of the different climb scenarios

Constant CAS Segment (kts)	Cruise Altitude (ft)	Cruise Mach Number
260 – 320	30.000 – 35.000	0.72 – 0.78

By generalizing these observations to ten different scenarios by varying the parameters from Table. 2, it was found that the minimum time climb strategy reduces climb time by 0.43% to 1.89% compared to the reference configuration (Fig. 12). Conversely, the strategy maximizing ground distance results in a longer climb time by 0.89% to 2.28%.

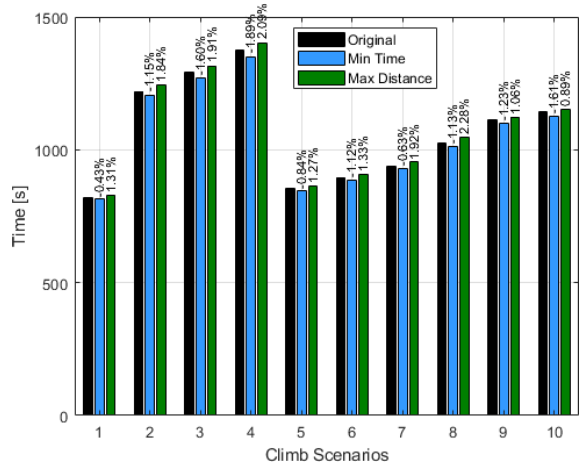

Fig. 12 Climb time results for 10 scenarios with the CRJ700 equipped with adaptive winglets

Climb optimization based on the mission objective also affects fuel consumption. The minimum time strategy reduces fuel consumption by 0.3% to 1.24% (Fig. 13), while the horizontal distance strategy leads to an increase of fuel consumption 1.36% to 2.38%. However, this approach enables a 1.07% to 2.67% greater ground distance before reaching cruise altitude, which may improve overall speed (Fig. 14).

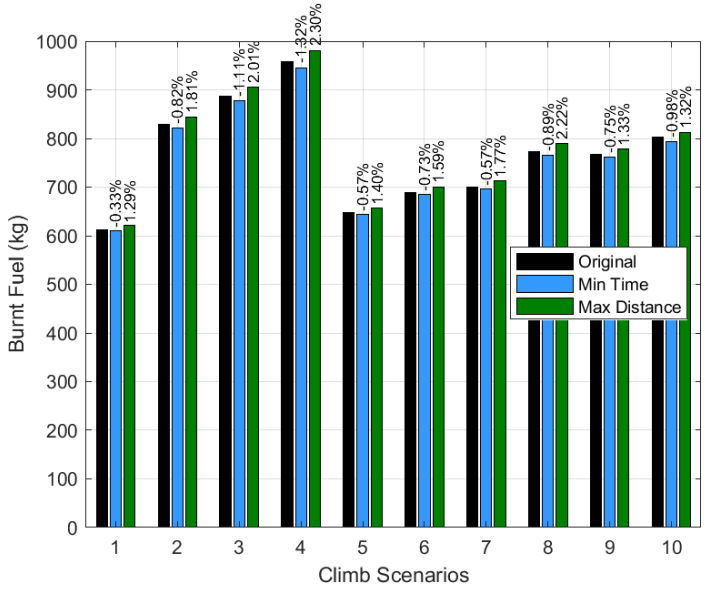

Fig. 13 Fuel consumption results for 10 climb scenarios with the CRJ700 equipped with adaptive winglets

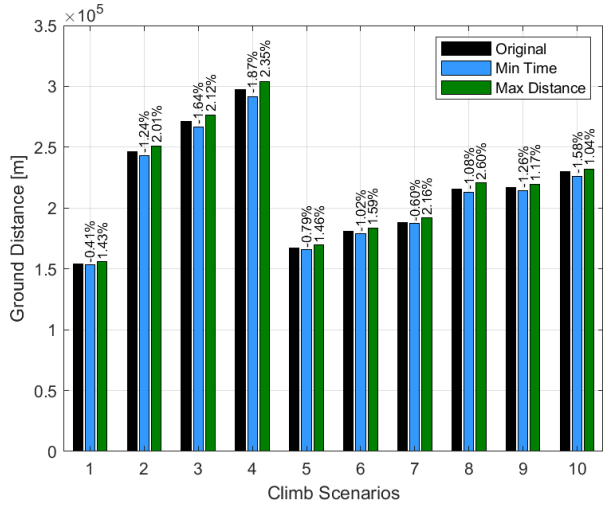

Fig. 14 Ground distance results for 10 climb scenarios with the CRJ700 equipped with adaptive winglets

To obtain statistically significant results, 50 scenarios were evaluated (Table. 3). In this table, Δ represents the obtained parameters difference with those of the reference model, and $\Delta\%$ the relative difference. This statistical analysis showed that adaptive winglets either reduce climb time and fuel consumption or increase the ground distance traveled, depending on the adopted strategy.

Table 3 Performance parameters differences for the CRJ700 equipped with adaptive winglets compared to fixed winglets

	Minimum Time	**Maximum Ground Distance**
Δt_s	−15.93±7.92s	15.89±6.70s
$\Delta t\%$	−1.23 ±0.40%	1.51 ±0.51%
Δd_{km}	−3.338±1.740km	3.61 ± 1.63 km
$\Delta a\%$	−1.25 ± 0.39%	1.68 ± 0.57%
ΔC_b	−7.56±3.48 kg	12.56 ± 4.49 kg
$\Delta C_b\%$	−0.84 ±0.27%	1.64 ± 0.44%

These results demonstrate the potential of adaptive winglets to optimize climb performance of the CRJ-700 based on their operational priorities. By dynamically adjusting its twist angle, the aircraft can either reach cruise altitude faster with lower fuel consumption or maximize climb distance to improve overall trip speed.

2. Cruise Results

The cruise phase performance simulations showed relatively small gains in fuel consumption when the winglet twist angle was optimized compared to the original configuration. The relative fuel consumption difference ranged between 0.1% and 0.4% for various aircraft weight configurations.

These results are shown in Fig. 15, where each bar corresponds to a relative fuel consumption difference as a function of altitude and Mach number for different weight values (50,000 lb, 60,000 lb, and 70,000 lb). Simulations covered a Mach range from 0.72 to 0.78 and altitudes from 30.000 ft to 35.000 ft.

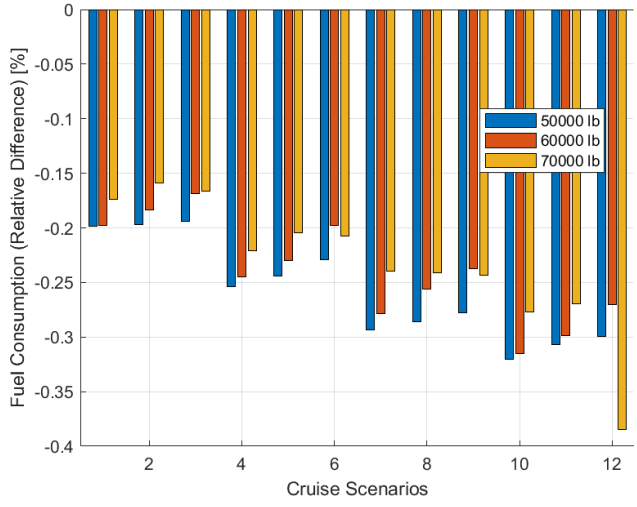

Fig. 15 Relative fuel consumption difference between the optimized and original configuration during cruise phases

In summary, the optimization led to a small improvement in fuel consumption, which was expected given that the original winglet was already designed optimally for the cruise phase.

3. Combined Climb and Cruise Results

The results obtained for different scenarios were evaluated by combining the climb and cruise phases over a total distance of 900 km. Figure 16 shows the simulated trajectories for the reference fixed-winglet configuration.

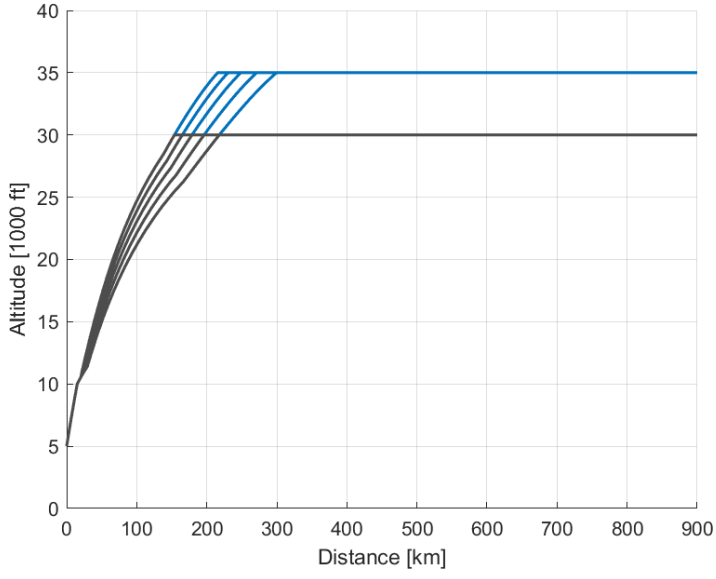

Fig. 16 Simulated flight trajectories for the combination of climb and cruise phases

Figures 17 and 18 present the differences in fuel consumption and flight duration obtained between the simulations with fixed and adaptive winglets for the climb time minimization and maximum ground distance strategies.

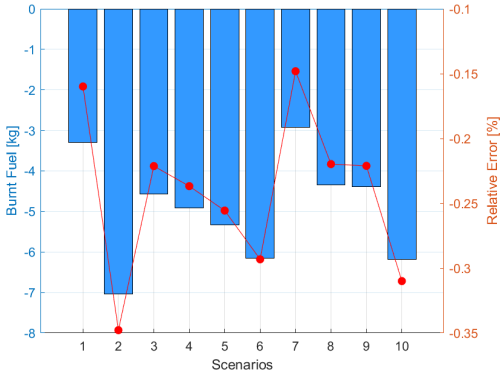

(a) Fuel consumption difference

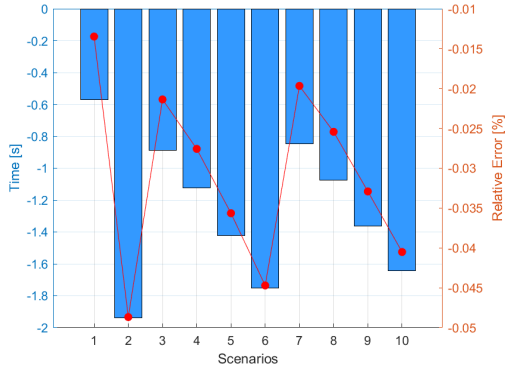

(b) Duration difference

Fig. 17 Simulation results for the minimum climb time strategy

For the minimum climb time strategy (Fig. 17), the relative time difference ranges from -0.05% to -0.01%, with an average of -0.03%.

Fuel consumption shows an average reduction of -0.23%, with its variations ranging from -0.35% to -0.15%. This trend indicates that minimizing climb time also leads to fuel savings.

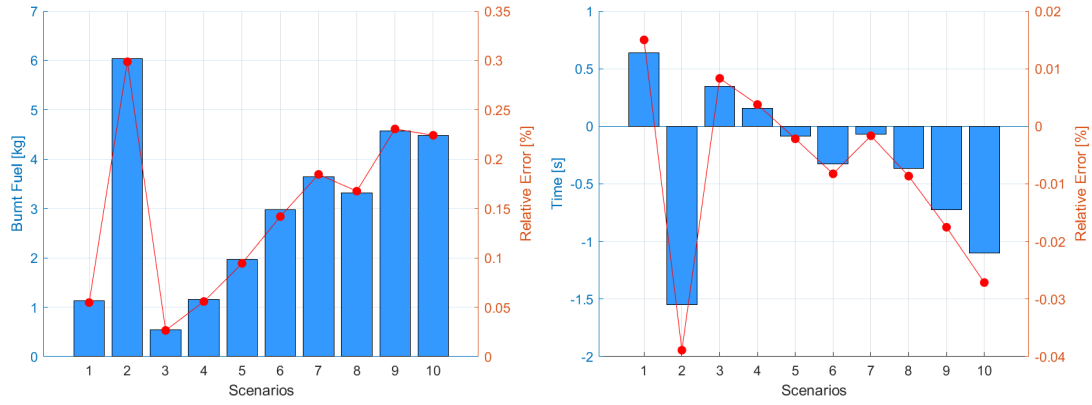

(a) Fuel consumption difference (b) Duration difference

Fig. 18 Simulation results for the maximum ground distance climb strategy

Regarding the strategy aiming to maximize ground distance (Fig. 18), its effect on duration is minimal, with a relative average variation of −0.01%, ranging from −0.04% to 0.02%. However, fuel consumption slightly increases on average by 0.14% with its variations from 0.03 % to 0.30%. This fact shows that although this approach optimizes distance, it leads to an increased fuel usage.

In conclusion, the minimum climb time strategy achieves noticeable fuel savings. However, the maximum distance strategy, which aims for a slightly faster overall trip, offers very small improvements at the cost of significantly higher fuel consumption, making it ultimately less attractive.

IV. CONCLUSIONS

The study presented in this article has demonstrated the potential of adaptive winglets use with variable twist angle to improve the aerodynamic and energy performance of the Bombardier CRJ700. The study highlighted the significant impact of twist angle variation on lift and drag, with notable benefits during the climb phase and moderate fuel savings during cruise.

A detailed CFD model was developed and validated using experimental data, showing that the optimal twist angle depends on the flight regime. While drag reductions are small at low Mach numbers, they reach up to 0.4% at higher Mach numbers. The lift increases with twist angle, with a maximum gain of about 0.5%.

The performance model used allowed the quantification of these gains: climb time reductions of up to 1.89%, fuel savings of up to 1.24%, or horizontal distance gains of up to 2.67%, depending on the optimization strategy. During cruise, fuel consumption was reduced by up to 0.4%.

In conclusion, this study confirms the relevance of variable twist winglets for enhancing the aerodynamic efficiency of regional aircraft and paves the way for more efficient aviation, better adapted to real flight conditions.

REFERENCES

[1] C. Queirolo and M. Andrés, *Impact of Morphing Winglets on Aircraft Performance*, 2018. URL https://repository. tudelft.nl/islandora/object/uuid%3A86a76d02-70f8-4468-a805-40ab4900b1a0.

[2] M. Segui, *CRJ700 Regional Aircraft Performances Optimization Using Adaptive Winglet Systems*, Ph.D. thesis, École de technologie supérieure, Jun. 2022.

[3] E. Kaygan and A. Gatto, Investigation of Adaptable Winglets for Improved UAV Control and Performance, *International Journal of Aerospace and Mechanical Engineering*, Vol. **8**, No. 7, 2014.

[4] K. Takenaka, K. Hatanaka, W. Yamazaki and K. Nakahashi, Multidisciplinary Design Exploration for a Winglet, *Journal of Aircraft*, Vol. **45**, No. 5, 2008, pp. 1601–1611. https://doi.org/10.2514/1.33031, URL https://arc.aiaa.org/doi/10.2514/1.33031.

[5] M. Segui, F. Abel, R. Botez and A. Ceruti, High-fidelity aerodynamic modeling of an aircraft using OpenFoam – application on the CRJ700, *The Aeronautical Journal*, Vol. **126**, No. 1298, 2022, pp. 585–606. https://doi.org/10.1017/aer.2021.86, URL https://www.cambridge.org/core/product/identifier/S0001924021000865/type/journal_article.

[6] J. Weierman and J. Jacob, Winglet Design and Optimization for UAVs, *American Institute of Aeronautics and Astronautics*, Chicago, Illinois, 2010. https://doi.org/10.2514/6.2010-4224, URL https://arc.aiaa.org/doi/10.2514/6.2010-4224.

[7] P. Panagiotou, S. Antoniou and K. Yakinthos, Cant angle morphing winglets investigation for the enhancement of the aerodynamic, stability and performance characteristics of a tactical Blended-Wing-Body UAV, *Aerospace Science and Technology*, Vol. **123**, 2022, p. 107467. https://doi.org/10.1016/j.ast.2022.107467, URL https://www.sciencedirect.com/science/ article/pii/S1270963822001419.

[8] M. P. Bakhai, S. B. Mat and N. A. B. Musa, Aerodynamics of a wing body with different Winglet Cant Angle, *E3S Web of Conferences*, Vol. **477**, 2024, p. 00029. https://doi.org/10.1051/e3sconf/202447700029, URL https://www.e3s-conferences.org/ articles/e3sconf/abs/2024/07/e3sconf_star2024_00029/e3sconf_star2024_00029.html, publisher: EDP Sciences.

[9] F. M. White, *Viscous Fluid Flow*, 3rd ed., McGraw-Hill Higher Education, New York, NY, 2006.

[10] W. Blake, T. P. T. Group and F. O. Engineering, *Jet Transport Performance Methods*, D6-1420, Boeing Company, Seattle, Washington, USA, 2009.

[11] G. Ghazi, R. M. Botez, C. Bourrely and A.-A. Turculet, Method for Calculating Aircraft Flight Trajectories in Presence of Winds, *Journal of Aerospace Information Systems*, Vol. **18**, No. 7, 2021, pp. 442–463. https://doi.org/10.2514/1.I010879.

[12] G. Ghazi and R. M. Botez, Method to Calculate Cessna Citation X Aircraft Climb and Cruise Trajectory using an Aero- Propulsive Model, *American Institute of Aeronautics and Astronautics*, Denver, Colorado, USA, 2017. https://doi.org/10.2514/ 6.2017-3550.

[13] G. Ghazi, R. M. Botez and N. Maniette, Cessna Citation X Takeoff and Departure Trajectories Prediction in Presence of Winds, *Journal of Aerospace Information Systems*, Vol. **17**, No. 12, 2020, pp. 659–681. https://doi.org/10.2514/1.I010854.

[14] J. Guerrero, M. Sanguineti and K. Wittkowski, CFD Study of the Impact of Variable Cant Angle Winglets on Total Drag Reduction, *Aerospace*, Vol. **5**, No. 4, 2018, p. 126. https://doi.org/10.3390/aerospace5040126, URL https://www.mdpi.com/ 2226-4310/5/4/126, number: 4 Publisher: Multidisciplinary Digital Publishing Institute.

[15] A. V. Popov, M. Labi, J. Fays and R. M. Botez, Closed-Loop Control Simulations on a Morphing Wing, *Journal of Aircraft*, Vol. **45**, No. 5, 2008, pp. 1794–1804. https://doi.org/10.2514/1.37073.

[16] A. V. Popov, T. L. Grigorie, R. M. Botez, Y. Mébarki and M. Mamou, Modeling and Testing of a Morphing Wing in Open-Loop Architecture, *Journal of Aircraft*, Vol. **47**, No. 3, 2010, pp. 917–926. https://doi.org/10.2514/1.46480.

[17] A. Koreanschi, O. Sugar Gabor, J. Acotto, G. Brianchon, G. Portier, R. M. Botez, M. Mamou and Y. Mebarki, Optimization and design of an aircraft's morphing wing-tip demonstrator for drag reduction at low speed, Part I – Aerodynamic optimization using genetic, bee colony and gradient descent algorithms, *Chinese Journal of Aeronautics*, Vol. **30**, No. 1, 2017, pp. 149–163. https://doi.org/https://doi.org/10.1016/j.cja.2016.12.013, URL https://www.sciencedirect.com/science/article/pii/ S1000936116302321.

[18] A. Koreanschi, O. Sugar-Gabor and R. M. Botez, Drag optimisation of a wing equipped with a morphing upper surface, *The Aeronautical Journal*, Vol. **120**, No. 1225, 2016, p. 473–493. https://doi.org/10.1017/aer.2016.6.

[19] T. L. Grigorie, S. Khan, R. M. B. M. Mamou and Y. Mebarki, Design and experimental testing of a control system for a morphing wing model actuated with miniature BLDC motors, *Chinese Journal of Aeronautics*, Vol. **33**, No. 4, 2020, pp. 1272–1287. https://doi.org/https://doi.org/10.1016/j.cja.2019.08.007.